Mesenchymal Stem Cell Targeting of Microscopic Tumors and Tumor Stroma Development Monitored by Noninvasive *In vivo* Positron Emission Tomography Imaging

Shih-Chieh Hung,[1,3,5,6] Win-Ping Deng,[2] Wen K. Yang,[1,6] Ren-Shyan Liu,[4,5] Chien-Chih Lee,[2] Tzu-Chi Su,[1,6] Rue-Jen Lin,[1,6] Den-Mei Yang,[1,6] Chi-Wei Chang,[4] Wei-Hong Chen,[2] Hon-Jian Wei,[2] and Juri G. Gelovani[7]

Abstract The aim of this study was to assess the efficacy human mesenchymal stem cells (hMSC) for targeting microscopic tumors and suicide gene or cytokine gene therapy. Immunodeficient mice were transplanted s.c. with human colon cancer cells of HT-29 Inv2 or CCS line, and 3 to 4 days later, i.v. with "tracer" hMSCs expressing herpes simplex virus type 1 thymidine kinase (*HSV1-TK*) and enhanced green fluorescent protein (*EGFP*) reporter genes. Subsequently, these tumors were examined for specificity and magnitude of HSV1-TK$^+$, EGFP$^+$ stem cell engraftment and proliferation in tumor stroma by *in vivo* positron emission tomography (PET) with ^{18}F-labeled 9-(4-fluoro-3-hydroxymethylbutyl)-guanine ([^{18}F]-FHBG). *In vivo* PET images of tumors growing for 4 weeks showed the presence of HSV1-TK$^+$ tumor stroma with an average of 0.36 $\pm$ 0.24% ID/g [^{18}F]-FHBG accumulation. *In vivo* imaging results were validated by *in situ* correlative histochemical, immunofluorescent, and cytometric analyses, which revealed EGFP expression in vWF$^+$ and CD31$^+$ endothelial cells of capillaries and larger blood vessels, in germinal layer of dermis and hair follicles proximal to the s.c. tumor site. These differentiated HSV1-TK$^+$, GFP$^+$ endothelial cells had limited proliferative capacity and a short life span of <2 weeks in tumor fragments transplanted into secondary hosts. We conclude that hMSCs can target microscopic tumors, subsequently proliferate and differentiate, and contribute to formation of a significant portion of tumor stroma. PET imaging should facilitate clinical translation of stem cell–based anticancer gene therapeutic approaches by providing the means for *in vivo* noninvasive whole-body monitoring of trafficking, tumor targeting, and proliferation of HSV1-tk-expressing "tracer" hMSCs in tumor stroma.

Authors' Affiliations: [1]Institute of Biomedical Sciences, Academia Sinica, Nankang; [2]Institute of Biomedical Materials, Taipei Medical University; Departments of [3]Medical Research, Orthopedics, and [4]Nuclear Medicine and National PET Cyclotron Center, Veterans General Hospital-Taipei; [5]School of Medicine, National Yang-Ming University, Taipei, Taiwan; and [6]Laboratory of Cell/Gene Therapy, China Medical University Hospital, Taichung, Taiwan; [7]Department of Experimental Diagnostic Imaging, University of Texas M.D. Anderson Cancer Center, Houston, Texas

Received 4/22/05; revised 7/19/05; accepted 8/8/05.

Grant support: Department of Health, Taiwan NCS-DOH Frontier Science grant DOH-92-TD.1050 (W.K. Yang); Veterans General Hospital-Taipei grants 92-376-1 (S-C. Hung); National Science Council grant NSC-91-2314-B-075-041 (S-C. Hung); Taiwan micro-PET imaging core project grant NSC-91-3112-P-075-001-y (W-P. Deng and R-S. Liu).

The costs of publication of this article were defrayed in part by the payment of page charges. This article must therefore be hereby marked *advertisement* in accordance with 18 U.S.C. Section 1734 solely to indicate this fact.

Note: S-C. Hung is a visiting scholar. W.K. Yang is a NSC Special Medical Chair Fellow at Academia Sinica, Taipei, Taiwan. J. Gelovani is the principle investigator of the U.S. Department of Energy grant DE-FG02-03ER63693 on PET Imaging of Adoptive Progenitor Cell Therapies.

S-C. Hung and W-P. Deng contributed equally to this work.

Requests for reprints: Juri G. Gelovani, Department of Experimental Diagnostic Imaging, University of Texas M.D. Anderson Cancer Center, Unit 057, 1515 Holcombe Boulevard, Houston, TX 77030. Phone: 713-563-3343; Fax: 713-563-4894; E-mail: jgelovani@mdanderson.org.

doi:10.1158/1078-0432.CCR-05-0876

Tumor progression involves tumor cell proliferation and infiltration into surrounding tissue and induction of different adaptive pathophysiologic and pathomorphologic processes in tissues that become involved in the developing tumor stroma. Tissue remodeling and neovascularization are critical processes in tumor stroma development (1). Recent studies have identified three main mechanisms of tumor angiogenesis: (a) existing vessel co-option (2); (b) endothelial sprouting (3); and (c) systemic recruitment of bone marrow–derived progenitor cells, including endothelial and mesenchymal progenitor cells (4). Mesenchymal stem cells (MSC) derived from bone marrow (5) are capable of self-renewal and differentiation into various somatic lineages (6). The *in vivo* plasticity of MSC has been used in novel therapeutic approaches to repair structural damage of the bone (7), central nervous system (8), skin (9), blood vessels (10), and myocardium (11).

Previous studies have shown that the adoptively transferred MSCs can migrate and engraft into the stroma of established tumor lesions (12). This phenomenon forms the basis for the paradigm of the "Trojan Horse" approach, in which the adult stem cells are used as shuttle vectors for delivery of gene therapies into growing tumors. If proven clinically effective, such an approach may in the future provide the means for therapy of metastatic tumors. However, from the clinical

perspective, it is critical to show that such an approach is not limited to radiologically and reliably detectable tumors but can also be used to target minimal residual disease and micrometastatic tumors. Therefore, in the current study, we aimed to investigate whether the MSCs after systemic i.v. administration will migrate and engraft into the microscopic tumor lesions during early stages of their development. Another question we explored was whether the proliferation of engrafted MSCs in the developing tumors can generate a significant fraction of tumor stroma, which could be subsequently eliminated with suicide gene therapy (e.g., HSV1-tk with ganciclovir), or provide the source for production of various antitumor cytokines, such as INF-β (12) or interleukin-2 (13).

To start addressing these questions, we used immortalized human MSCs (hMSC) that were lentivirally transduced with the herpes simplex virus type 1 thymidine kinase (HSV1-TK), and the *Aequorea victoria* enhanced green fluorescent protein (EGFP), under control of two separate promoters. As in the case of previously described *TKGFP* fusion reporter gene (14–17), the *EGFP* reporter gene facilitated the fluorescence-activated cell sorting–aided selection of transduced MSCs and their fluorescence microscopic visualization *in vitro* and *in situ*. The HSV1-TK reporter gene allowed for the repetitive molecular imaging with ^{18}F-labeled 9-(4-fluoro-3-hydroxymethylbutyl)-guanine ([^{18}F]-FHBG) micropositron emission tomography (micro-PET) for noninvasive *in vivo* whole-body monitoring of the migration, engraftment, and proliferation of i.v. administered MSCs into tumor stroma or other organs and tissues.

Both the noninvasive repetitive micro-PET imaging and the *in situ* analyses of tumor tissue samples revealed that hMSC localized to the sites of microscopic tumor lesions and participated in tumor stroma formation. The latter process included initial proliferation of hMSCs and their subsequent differentiation into vascular endothelial and other tumor stromal cells, as well as into different cellular components of peritumoral tissues (i.e., skin and hair follicles).

Materials and Methods

Tumor cells. The invasive variant of HT-29 Inv2 colon carcinoma cells was described in our previous study (18) using an *in vitro* Matrigel (BD Biosciences, San Jose, CA) invasion technique. The CCS line was established from a primary tumor of a 63-year-old female with Duke C_3 colon adenocarcinoma (Veteran Hospital, Taipei, Taiwan) and used within 30 *in vitro* passages. Both cell lines were grown in MEM containing 10 units/mL penicillin, 10 μg/mL streptomycin, 2 mmol/L glutamine, and 10% fetal bovine serum (Hyclone, Logan, UT), in 37°C humidified atmosphere with 5% CO_2.

Human mesenchymal stem cells. The hMSC line was originally cultured from the bone marrow of a 61-year-old female donor, immortalized by retroviral-mediated transduction of human papilloma virus *E6/E7* genes, and maintained in DMEM containing 1 mg/mL glucose and 10% fetal bovine serum of a selected lot (Invitrogen, Carlsbad, CA; ref. 19). This immortalized hMSC line is >99% positive for CD29, CD44, CD90, CD105, SH2, and SH3 MSC characteristic markers.

Lentiviral vector construction and transduction. The self-inactivating pTY-EFEGFP lentiviral vector backbone was originally developed and provided by Dr. Lung-Ji Chang (University of Florida, FL; ref. 20). The pTY-EFEGFP-TK vector, was constructed by inserting into the *HSV1-TK* gene driven by the *HSV1-tk* promoter into the *Kpn*I site of the pTY-EFEGFP vector that carries the *EGFP* reporter gene driven by the EF1α promoter. Procedures for DNA transfection of TE671 cells to produce packaged virus of pTY-EFEGFP-TK vector and for transduction of hMSC were previously described (21). Using the TE671 vector at a multiplicity of infection = 1, the EGFP expression was observed in close to 30% of hMSC. The transduced EGFP$^+$ (and HSV1-TK$^+$) hMSCs were separated using FACS Vantage (BD Biosciences) and designated TG-hMSC "tracer cells." Subsequently, the expression of HSV1-TK in TG-hMSCs was verified using *in vitro* radiotracer accumulation assay with [^{18}F]-FHBG (16, 22) and by an *in vitro* susceptibility test to ganciclovir (LD_{50} = 0.01 mmol/L) as previously described (23, 24). In contrast, nontransduced hMSCs and nontransduced human colon cancer cells were insensitive to ganciclovir at 1 mmol/L and showed negligible uptake and retention of [^{18}F]-FHBG *in vitro*. The proliferative rate of transduced and nontransduced hMSCs were similar.

Tumor xenografts in mice. Study protocols involving mice were developed in accordance with the American Association for Accreditation of Laboratory Animal Care guidelines and approved by the Institutional Animal Committee of Academia Sinica. Nonobese diabetic/severe combined immunodeficient mice were obtained from The Jackson Laboratory (Bar Harbor, ME) and maintained as a colony at the National Taiwan University Animal Facility (Taipei, Taiwan) in specific pathogen-free conditions. The mice were used for experiments at 6 to 10 weeks of age. HT-29 Inv2 or CSS tumor cells were injected s.c. at a dose of 10^6 per injection site with or without tracer TG-hMSCs, as will be described further. Tumor nodules usually became palpable within 1 week and reached about 4 to 6 mm in diameter in 4 weeks after s.c. cell injection.

Micropositron emission tomography imaging. The [^{18}F]-FHBG was prepared using no-carrier-added one-pot synthesis procedure, as previously described (25). Tumor-bearing mice under gas anesthesia (2% isoflurane/98% oxygen) were injected via tail vein with 230 to 250 μCi of [^{18}F]-FHBG in 0.2-mL sterile saline and imaged on a micro-PET R4 system (Concorde Microsystems, Inc., Knoxville, TN) at 4 hours after radiotracer injection. Axial PET images were acquired for 10 minutes in prone position of mice. The images were reconstructed by using two-dimensional ordered subsets expectation maximization, as previously described (26).

Histology and immunohistochemistry. In different study groups, selected mice were sacrificed after the end of PET imaging session by cervical dislocation. S.c. tumors were dissected from the surrounding soft tissues and fixed in 2% paraformaldehyde for fluorescent microscopy of EGFP (27). Alternatively, tissue sections were immunostained for EGFP expression using the rabbit anti-GFP polyclonal antibody (Clontech, Mountain View, CA) followed by horseradish-labeled goat anti-rabbit IgG antibody and finally processed for immunoperoxidase/3,3′-diaminobenzidine staining (Vector, Burlingame, CA) to facilitate the visualization of lower levels of EGFP expression.

PCR. The nuclear DNA extracts from cultured cells and tumor tissue samples were prepared using commercially available DNA isolation kit (Blood and Tissue Genomic Mini, Viogene, Sunnyvale, CA). PCR was done with EGFP primer pairs (sense, 5′-ATGAGCAAGGGCGAGGAACT-3′; antisense, 5′-TCACTTGTACAGCTCGTCCA-3′) by initial heating at 95°C for 5 minutes followed by 35 cycles of 95°C for 1 minute, 60°C for 1 minute, and 72°C for 1 minute, and a final elongation reaction at 72°C for 10 minutes. DNA products were separated by electrophoresis in 1% agarose gel, stained with ethidium bromide, and visualized under UV illumination.

Cytofluorometry. Single-cell suspensions were obtained from the aseptically minced tumor fragments by collagenase digestion in 15 volumes per wet weight of Hank's balanced solution containing 1 mg/mL collagenase and 2 mmol/L EDTA overnight at 4°C. The fractionated cells were washed with PBS and used directly or cryopreserved in FCS/DMSO (9:1, v/v) at −80°C before analysis. The washed cells, with or without fixation/permeabilization, were reacted with rabbit anti-GFP polyclonal antibody (Clontech) plus FITC-labeled donkey anti-rabbit IgG antibody or FITC-labeled anti-GFP; mouse anti-human von Willebrand factor (hvWF; Immunotech, Westbrook, ME) plus PE-labeled goat

anti-mouse IgG antibody or PE-labeled anti-hvWF; and PE-labeled mouse monoclonal antibodies against human CD14 (PharMingen, San Diego, CA), CD31, CD90, CD105 (Serotec, Raleigh, NC), and smooth muscle actin (Chemicon, Temecula, CA). Isotype control antibodies were used in parallel to set negative gates. The cells were analyzed on a FACS Vantage cytofluorometer using Cell Quest software (BD Biotech, Research triangle Park, NC).

Results

Micropositron emission tomography imaging of human mesenchymal stem cell targeted tumors. In the *first group* of mice (n = 6), we assessed the ability of the MSCs coimplanted with tumor cells to proliferate inside the growing tumor lesions and contribute to the development of tumor stroma. In this group, two s.c. tumor xenografts were established by s.c. injection of a mixture of 1×10^6 HT-29 Inv2 cells and 5×10^5 tracer TG-hMSCs (HT-29 + TG-hMSC) into the right flank, and by s.c. injection of 1×10^6 HT-29 Inv2 cells alone (HT-29) into the left flank. The micro-PET imaging with [^{18}F]-FHBG was done 4 weeks later and showed a profound uptake and retention of the radiotracer in HT-29 + TG-hMSC tumors (5.78 ± 4.79% ID/g), indicating persistent HSV1-TK expression by the tracer TG-hMSC-derived tumor stroma (Fig. 1A). In contrast, no [^{18}F]-FHBG uptake and retention above body background was observed in the contralateral HT-29 tumors, which served as negative control.

In the *second group* of mice (n = 6), only one tumor xenograft per mouse was established by s.c. injection of 1×10^6 HT-29 Inv2 cells into the right flank. In this group, 5×10^5 tracer TG-hMSCs were administered through the tail vein 3 days after s.c. tumor injection. In this group, micro-PET imaging studies confirmed the ability of i.v. administered tracer TG-hMSCs to migrate to the sites of microscopic tumor

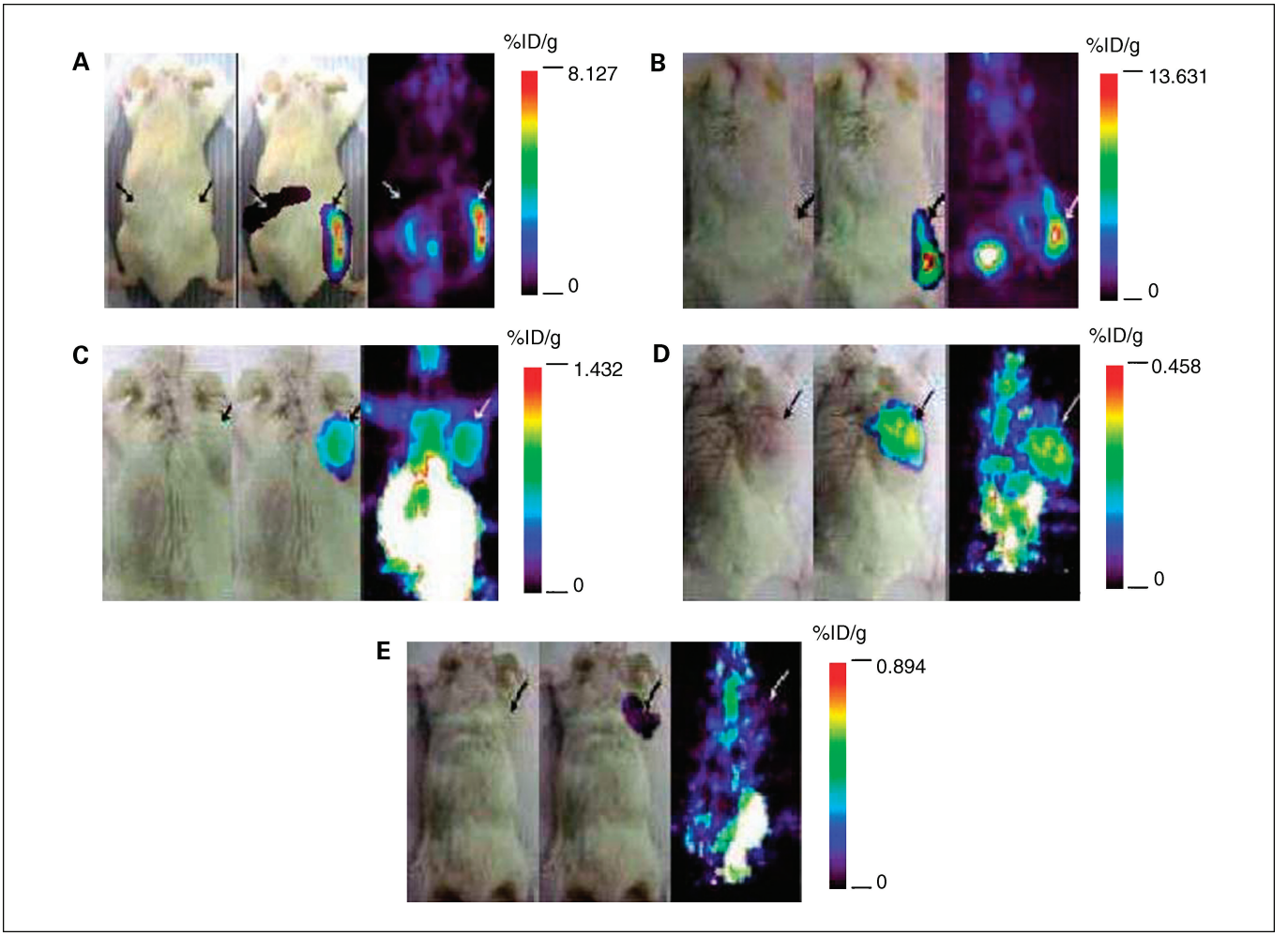

Fig. 1. Micro-PET imaging of tumors developed from human colon cancer cells with or without s.c. coinjection of tracer TG-hMSCs into nonobese diabetic/severe combined immunodeficient mice. *A,* a mouse 30 days after inoculation of 1×10^6 HT-29 Inv2 cancer cells plus 5×10^5 TG-hMSCs [HT-29 (s.c.) + TG-hMSC (s.c.) tumors] in the right flank and 1×10^6 HT-29 Inv2 alone [HT-29 (s.c.) tumors] in the left flank. One hour after i.v. injection of 0.25 mCi [^{18}F]-FHBG, the micro-PET images showed [^{18}F]-FHBG retention in the HT-29 (s.c.) + TG-hMSC (s.c.) tumors but not in the contralateral HT-29 (s.c.) tumors. Arrows, locations of the tumors. *B,* a mouse 30 days after s.c. injection of HT-29 and 27 days after tail vein infusion of TG-hMSC [HT-29 (s.c.) + TG-hMSC (i.v.) tumors]. Micro-PET image of [^{18}F]-FHBG retention was observed in HT-29 (s.c.) + TG-hMSC (i.v.) tumors at 3 hours after [^{18}F]-FHBG infusion. *C* and *D,* micro-PET images of mice, which were injected s.c. with 2×10^6 CCS colon cancer cells, and 3 days later, injected i.v. with 5×10^5 TG-hMSC. The mice were imaged with [^{18}F]-FHBG and micro-PET, which showed an increase in [^{18}F]-FHBG accumulation in tumors between 18 days (*C*) and 30 days (*D*) of tumor growth. *E,* micro-PET image showing no significant [^{18}F]-FHBG retention in a secondary tumor formed in a new nonobese diabetic/severe combined immunodeficient mouse host at 4 weeks after transplantation of minced CCS (s.c) + TG-hMSC (i.v.) tumor fragments obtained from the mouse in (*D*). Images contrasted to better highlight the distribution of signal in tumors (*B-D*). Therefore, relatively high radioactivity levels are observed in the abdominal areas in mice represents a normal pattern of hepatobiliary to intestinal clearance of [^{18}F]-FHBG.

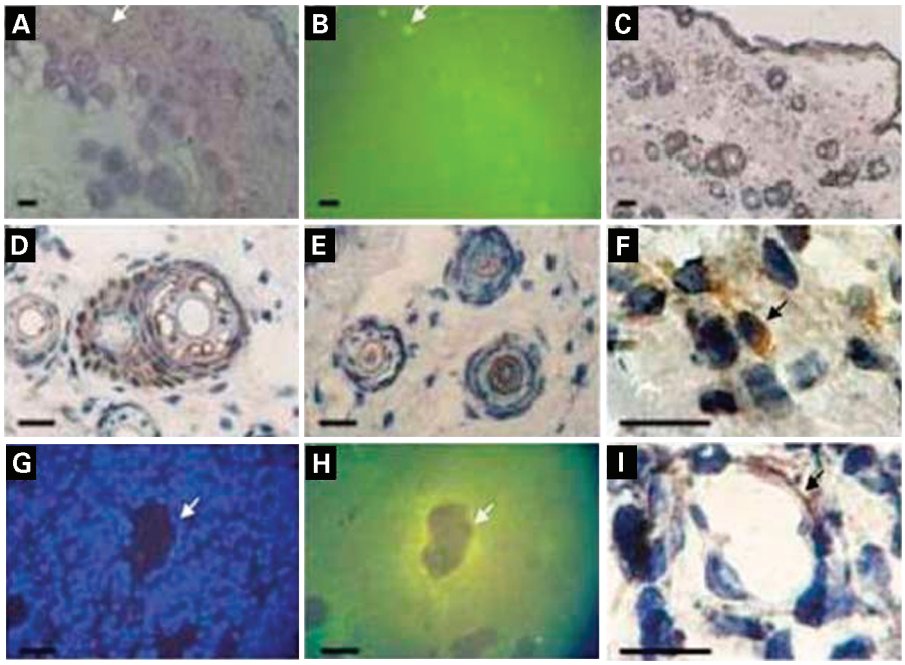

Fig. 2. Histologic characterization of EGFP-expressing cells in tumors developed from s.c. injection of HT-29 Inv2 cells and tracerTG-hMSC in nonobese diabetic/severe combined immunodeficient mice [HT-29 (s.c.) + TG-hMSC (s.c.) tumors]. Light microscopy (magnification, ×20) of the H&E-stained sections of HT-29 (s.c.) + TG-hMSC (s.c.) tumors at 30 days of growth (*A*). The distribution of $EGFP^+$ fluorescent cells in adjacent sections examined by fluorescence microscopy (*B* and *H*) and immunoperoxidase (*C, D, E, F,* and *I*). Numerous EGFP-positive cells were detected in the periphery of tumors (*A-C*) and in hair follicles (*D* and *E*). Toward the inner tumor, the GFP-positive cells were fewer and occasionally observed in the tumor stroma (*F*) but were often restricted to small vessels (*G*, 4′,6-diamidino-2-phenylindole stain of area *H*) and dispersed within the parenchyma. At higher magnification, the GFP-positive cells appeared as small or elongated mononuclear cells, with vascular endothelial cell – like morphology, lining the inner walls of small vessels and forming capillaries (*I*). Bar, 20 μm.

lesions, engraft into these microscopic tumor lesions, and contribute to the development of a significantly portion of tumor stroma (Fig. 1B).

Similar results were observed in tumors produced from human colon adenocarcinoma cell line, CCS. Micro-PET images obtained at different days after s.c. injection of tumor cells showed the initial migration of i.v. administered tracer TG-hMSC to the sites of s.c. CCS tumor cell injection. Repetitive micro-PET imaging done at 15 and 27 days after tracer TG-hMSCs injection (18 and 30 days of tumor growth) showed exponentially increasing [^{18}F]-FHBG accumulation at the sites of s.c. CCS tumor cell injection (Fig. 1C and D), which is indicative of tracer TG-hMSC proliferation and significant contribution to growing tumor stroma development.

In the *third group* of mice (n = 6), we aimed to determine whether the tracer hMSC-derived tumor stromal cells retain stem cell properties (i.e., the capacity for self-renewal). To address this question, we obtained tumor tissue samples at the end of a 30-day imaging study conducted in the second group of animals and implanted s.c. aseptically minced tumor fragments of about 2 mm in diameter into the new nonobese diabetic/severe combined immunodeficient mouse recipients. Four weeks later, the recipient mice developed s.c. tumors and were imaged with [^{18}F]-FHBG PET, which showed the lack of radiotracer uptake above the body background levels (Fig. 1E), which is indicative of a very low density or a lack of tracer TG-hMSCs progeny inside newly developed tumor stroma.

Microscopic analyses of tumor stroma and surrounding tissues. To validate the results of noninvasive *in vivo* micro-PET imaging and to further characterize the type of cellular elements in tumor stroma, we examined tumor tissue sections obtained in all groups of animals for the type of cells expressing EGFP. In the first group of mice with s.c. coinjection of tumor cells and tracer TG-hMSCs, as well as in the second group with i.v. administration of tracer TG-hMSCs, the EGFP fluorescence and immunostaining were detectable mainly in cells forming the capillary-like structures (Fig. 2A, B, G, H, and I), in the cells within the inner layer of small arterioles (Fig. 2B and C), and in connective tissue cells (Fig. 2F). These results show that both i.t. coadministered as well as i.v. administered tracer TG-hMSCs contributed significantly to the development of vascular and connective tissue components of tumor stroma growing in nonobese diabetic/severe combined immunodeficient mice.

Surprisingly, a relatively large number of tracer TG-hMSCs were detected the skin adjacent to and overlaying the s.c. tumors. In particular, EGFP-expressing cells were identified in hair follicles, the basal layer of dermis, and in the endothelial and intimal layers of small blood vessels in the skin overlaying s.c. tumors (Fig. 3).

In situ *validation of positron emission tomography imaging of tracer human mesenchymal stem cell proliferation in tumors.* To validate micro-PET imaging results and to quantitate the magnitude of tracer TG-hMSCs proliferation in tumors in different study groups, fresh tumor tissue samples were gradually digested to obtain single-cell suspensions containing both the tumor and stromal cell fractions. The numbers of $EGFP^+$ cells were assessed by cytofluorometry and plotted over time (days of tumor growth *in vivo*; Fig. 4). Because only 5×10^5 tracer hMSCs were initially administered either by coimplantation or by i.v. injection, these data indicate that tracer TG-hMSCs had proliferated at least several times during the tumor stroma development. This was more evident when the cell numbers were fitted with an exponential function. The rates of tracer TG-hMSC-derived progeny cell proliferation were similar in different study groups independent of the mode of administration. The average doubling time of tracer

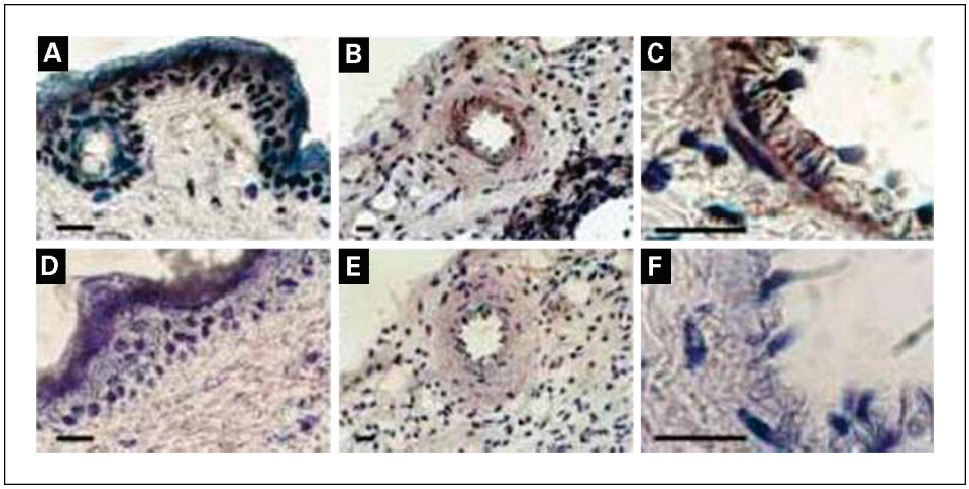

Fig. 3. The morphology of 30-day HT-29 (s.c.) + TG-hMSC (i.v.) tumors. Numerous EGFP-containing cells revealed by immunoperoxidase staining were located mainly within dermis and hair follicles of the skin overlaying the s.c. tumors (*A*) and also diffusely present in the inner wall of small arteries but not in the smooth muscle layers (*B*). At higher magnification, the cells had small and ellipsoid nuclei, characteristic of the vascular endothelial cells (*C*). Adjacent tissue sections stained with the omission of the anti-GFP antibody were used as negative controls (*D-F*). Bar, 20 μm.

TG-hMSCs was 6.51 ± 0.36 days, as determined by dividing the ln(2) by the coefficients of exponential fits of data. The levels of micro-PET detectable [^{18}F]-FHBG radioactivity concentration in CCS (s.c.) + TG-hMSCs (i.v.) tumors increased exponentially between days 17 and 30 and paralleled increasing numbers of EGFP$^+$ cells in the growing tumors.

The sensitivity of micro-PET imaging of tracer TG-hMSCs could be calculated by dividing the number of recovered GFP$^+$ cells from s.c. tumors by the corresponding tumor volume. For example, dividing 3.2×10^6 TG-hMSCs recovered from the day 18 CCS (s.c.) + TG-hMSCs (i.v.) tumors by their volume of about 120 mm^3, results in 2.6×10^4 cells/mm^3, that were reliably detectable by the micro-PET R4 after injection of 250 μCi [^{18}F]-FHBG per animal. Because the micro-PET R4 can detect at least a 10- to 20-fold lower levels of radioactivity concentration, we can reliably extrapolate that the lower threshold of micro-PET imaging is close to 1,000 cells/mm^3.

In situ *quantitation of TG-hMSC progeny cells and cell surface markers.* *In situ* characterization of EGFP$^+$ cells in HT-29 (s.c.) + TG-hMSC (i.v.) tumors involved PCR amplification of EGFP sequence (717 bp) using 1 μg of cellular DNA prepared from digestion-aided disaggregates of HT-29 (s.c.) + TG-hMSC (i.v.) tumors and HT-29 (s.c.) tumors. In HT-29 (s.c.) + TG-hMSC (i.v.) tumors, the *EGFP* gene was barely detectable in readily dissociated, loose tumor cell fractions, but was abundant in the stromal cell fraction. In contrast, the *EGFP* gene was not detectable in tumors established from HT-29 cells only, without coadministration of TG-hMSCs. The TG-hMSC and HT-29 tumor cells were used as positive and negative controls, respectively (Fig. 5A).

Cytofluorometric analysis of HT-29 (s.c.) + TG-hMSC (i.v.) tumors showed that 11.5% of all cells were EGFP$^+$ (Fig. 5B). We then used antibodies against various human cell surface markers to analyze the phenotype of the EGFP$^+$ cells by immunocytofluorometry. An endothelial cell marker, vWF was found on about one third of the EGFP$^+$ cells of HT29 (s.c.) + hMSC (i.v.) tumors (Fig. 5C). Elevated levels of CD31 endothelial marker (28) expression but low and undetectable levels of CD90 and CD105 were observed in stromal matrix-associated EGFP$^+$ cells (Fig. 5C), although the CD90 and CD105 are known to be highly expressed in hMSCs (29). None of the EGFP$^+$ cells reacted with anti-human smooth muscle actin antibodies (data not shown). Thus, the targeted TG-hMSC had differentiated mainly into the endothelial but not the smooth muscle cell components in tumor angiogenesis, confirming prior immunohistochemical observations (Figs. 2 and 3).

Apparent loss of self-renewal capacity of differentiated tracer TG-hMSC-derived stromal cells. To determine if tumor-engrafted tracer hMSC-derived progeny stromal cells retain self-renewal capacity, we cultured *in vitro* the tumor and stromal cells obtained from digested tissue fragments of micro-PET positive CSS (s.c.) + hMSC (i.v.) tumors. After 5 days in culture, the EGFP$^+$ fluorescent cells were visible within

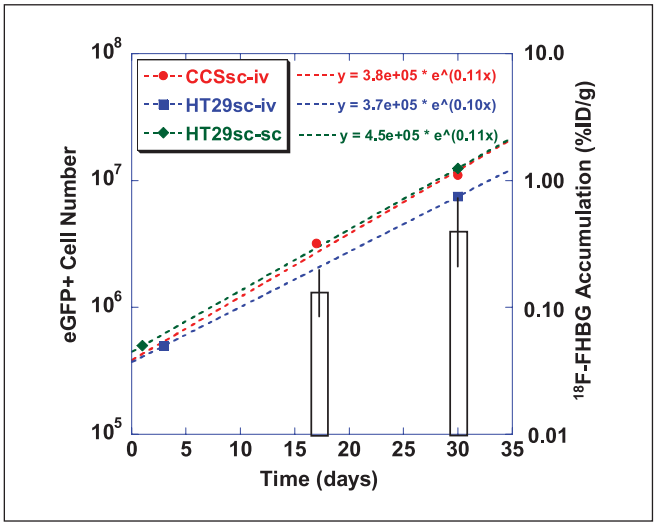

Fig. 4. *In situ* validation of *in vivo* proliferation of TG-hMSCs in tumors observed by micro-PET imaging. The numbers of EGFP$^+$ cells measured by fluorescence-activated cell sorting in digestion-aided disaggregates of whole tumors obtained at different days after coimplantation or i.v. injection of TG-hMSC are plotted over time (days of sampling): red circles, CCS (s.c.) + TG-hMSC (i.v.) tumors; blue squares, HT-29 (s.c.) + TG-hMSC (i.v.) tumors; green diamonds, HT-29 (s.c.) + TG-hMSC (s.c.) tumors. Points are fitted with an exponential regression function using 5×10^5 as the initial number of injected TG-hMSCs. Columns, levels of [^{18}F]-FHBG accumulation (%ID/g) in CCS (s.c.) + TG-hMSC (i.v.) tumors on 17 and 30 days of s.c. tumor growth.

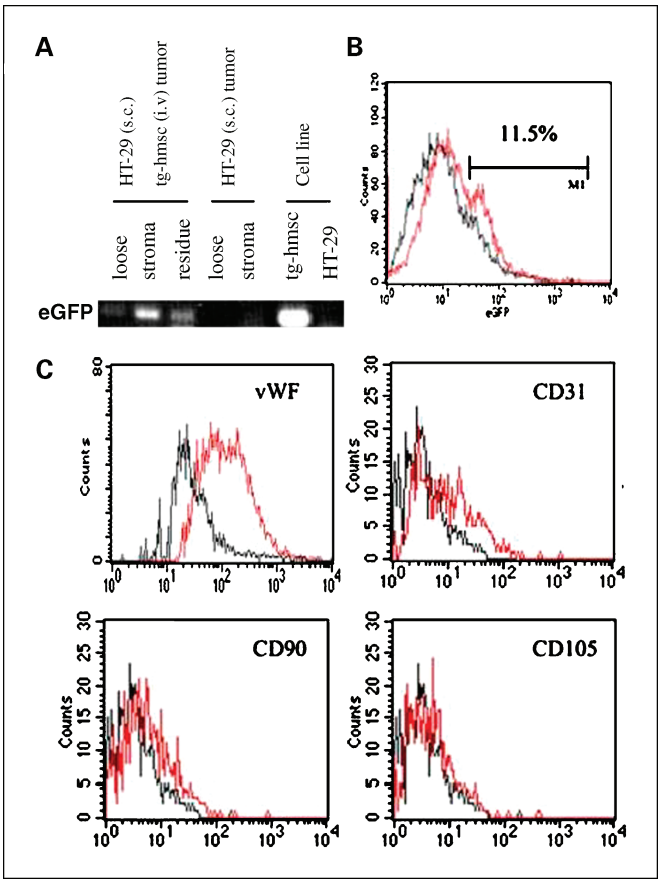

Fig. 5. *In situ* characterization of EGFP$^+$ cells in HT-29 (s.c.) + TG-hMSC (i.v.) tumors. *A,* agarose gel electrophoresis of PCR-amplified EGFP sequence (717 bp) done using 1 μg of cellular DNA prepared from loosely associated cell fraction (*loose*), stromal matrix associated fraction (*stroma*), and the residue (*residue*) of HT-29 (s.c.)/TG-hMSC (i.v.) tumor and HT-29 (s.c.) tumor, TG-hMSC, and HT-29 cells. *B,* cytofluorometric histograms comparing the stromal matrix cell fractions of HT-29 (s.c.) + TG-hMSC (i.v.) tumors (*red*) and HT-29 (s.c.) tumors (*black*), examined with anti-GFP specific antibody. EGFP$^+$ cells in the gated area represented 11.5% of total cells. *C,* histograms showing the presence of human endothelial cell markers but absence of hMSC markers in EGFP$^+$ cells obtained from the HT-29 (s.c.) + TG-hMSC (i.v.) tumor after 30 days of growth *in vivo*. Stromal matrix – associated cell fractions were double stained with FITC-labeled anti-GFP mouse monoclonal antibody, and with a PE-labeled anti-vWF, or anti-CD31, or anti-CD90, or anti-CD105 to assess the expression of these cell surface markers on EGFP$^+$ cells (*red*). PE-labeled mouse isotype immunoglobulins were included in parallel to serve as the negative control (*black*).

spheroid-like cellular clusters and flat colonies (Fig. 6A-D). The EGFP expression in these cultured cells was confirmed by immunocytofluorometry (Fig. 6E and F). However, these EGFP-expressing cells did not proliferate further under these culture conditions and were rapidly overgrown by the CCS colon cancer cells. These results are consistent with our observations with micro-PET imaging in experiments involving reimplantation of small tumor fragments into new recipient mice (the third study group; Fig. 1E).

Discussion

The aim of the current study was to assess whether the hMSCs can migrate and engraft into the microscopic tumors, subsequently proliferate and form a significant portion of developed tumor stroma. To achieve this aim, we used clinically applicable *in vivo* whole-body PET imaging with [^{18}F]-FHBG to noninvasively monitor the fate of genetically modified HSV1-TK- and EGFP-expressing "tracer" hMSCs (TG-hMSCs) upon their i.t. or i.v. administration. We use the term "tracer cells" in context of the potential future clinical scenario, in which the HSV1-TK-expressing hMSCs will be used to "trace" the coadministered therapeutic hMSCs genetically modified to express various anticancer cytokines (12, 13). Similar PET imaging approach was applied in several recent studies for noninvasively visualization of HSV1-TK-expressing stem cells after direct intramyocardial injection (30, 31) and for visualization of tumor targeting by the adoptively transferred tumor antigen-specific T cells (32, 33). Another potential clinical therapeutic protocol, which would be greatly facilitated by noninvasive imaging, would include repetitive (e.g., biweekly or monthly) administration of HSV1-TK-expressing autologous stem cells to patients following resection of a primary tumor, which has high likelihood of metastases that are radiologically not detectable at the time of resection. In case the local or distal metastases will be developing after resection of primary tumor, such repetitive administration of HSV1-TK-expressing stem cells would result in the development of HSV1-TK-expressing tumor stroma, which should be detectable with whole-body PET imaging. The HSV1-TK-expressing tumor stroma can be "eliminated" by treatment with ganciclovir, which should cause a significant regression of metastatic tumor lesions, the efficacy of which can be assessed by conventional

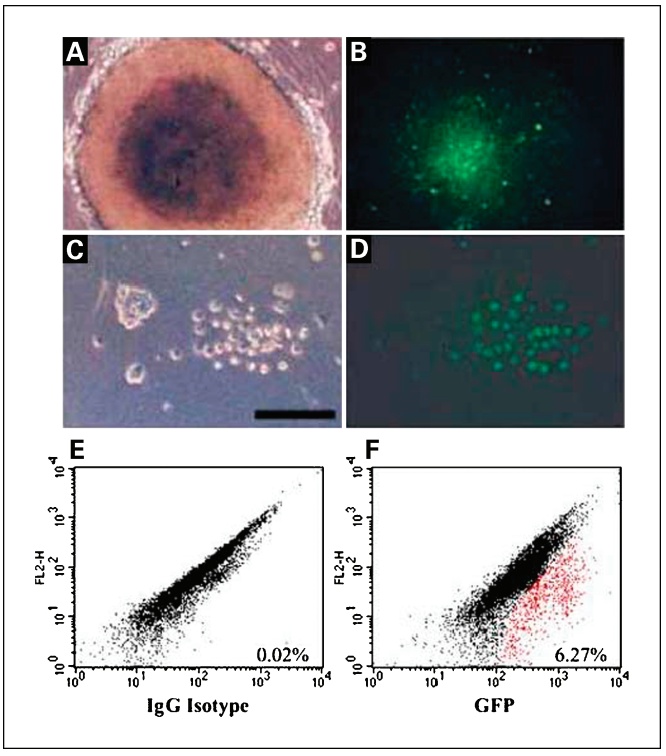

Fig. 6. *In vitro* assessment of self-renewal capacity of differentiated tracer TG-hMSC-derived stromal cells. The morphology of digestion-aided disaggregated tissue fragments of micro-PET positive CSS (s.c.) + hMSC (i.v.) tumors after 5 days in culture as seen by dark field microscopy (*A* and *C*) and fluorescence microscopy of EGFP (*B* and *D*). The EGFP$^+$ fluorescent cells are clearly visible within spheroid-like cellular clusters (*A* and *B*) and flat colonies (*C* and *D*). The EGFP expression in these cultured cells was confirmed by immunocytofluorometry using anti-eGFP antibody (*F*); the IgG isotype antibody was used for control (*E*).

anatomic computed tomography, magnetic resonance, and [^{18}F]-FDG imaging. Thereafter, the cycle of therapy with HSV1-tk-expressing stem cells followed by whole-body PET imaging of HSV1-tk expression and ganciclovir therapy could be repeated.

As the initial step of our studies, we assessed whether the micro-PET imaging with [^{18}F]-FHBG is sensitive and specific enough for the detection of HSV1-TK-expressing tumor stroma in s.c. tumors that had been established by s.c. coinjection of colon HT29 carcinoma cells and tracer hMSCs in mice. The sensitivity of micro-PET imaging with [^{18}F]-FHBG depends on the level of *HSV1-TK* reporter gene expression per cell and the number of HSV1-TK$^+$ cells within the minimum resolution volume of 2 × 2 × 2 mm for the Micro-PET R4 scanner (Concorde Microsystems). The calculated lower threshold of micro-PET R4 sensitivity in our *in vivo* imaging/*in situ* validation studies was close to 1,000 cells/mm^3, which is comparable with results reported previously, which estimated the lower threshold of Micro-PET R4 scanner sensitivity for imaging with [^{18}F]-FHBG sr39HSV1-TK-expressing cells as 10^6 cells per 0.1 mL (or 10^4 to 10^5/mm^3 of tissue; refs. 31, 34).

Next, we did *in vivo* PET imaging and *in situ* analyses at 15 and 27 days after i.v. administration of HSV1-TK$^+$, GFP$^+$ tracer hMSCs in mice with microscopic s.c. CCS tumors. We showed that these cells engrafted into the microscopic tumors, subsequently proliferated with a calculated average doubling time of 6.51 ± 0.36 days, and contributed to the formation of a significant fraction of tumor stroma. We observed similar micro-PET imaging results with other human xenografts in nonobese diabetic/severe combined immunodeficient mice, including A431 epidermoid carcinoma, Ova-3 ovarian carcinoma, and Taiwan domestic patient CZF pancreatic carcinoma (data not shown). Tumor-targeting properties of stem cells have been previously reported in glioblastoma model (35); in studies of tumor angiogenesis by hematopoietic stem cells (4), stem cells were used as vehicles for gene therapy of human colon cancer xenografts (12). Cancer cells are known to produce various growth factors that stimulate angiogenesis (36). In response to these factors, endothelial precursors including bone marrow–derived endothelial progenitors (10) and hematopoietic stem cells (4) may become recruited into tumor neovascularization process. Whether some of these factors possess chemotactic and/or selective differentiation-inducing activities for MSC remains to be investigated. It remains to be determined whether the endogenous MSCs are mobilized by the microscopic tumors from the bone marrow and migrate to sites of microscopic tumors, and what percentage of tumor stroma develops from the engrafted MSCs.

Because the radiotracer used in the current study was [^{18}F]-FHBG, which produces in mice a substantial abdominal background due to predominantly hepatobilliary routes of elimination, we are unable to definitively answer this question. The use of another radiotracer, [^{18}F]-FEAU, in our future studies will potentially enable us to address this question, because [^{18}F]-FEAU is eliminated by renal clearance and produces almost no nonspecific background radioactivity levels in all tissues and organs (except for residual activity in the bladder; ref. 37). Nevertheless, the use of [^{18}F]-FHBG in combination with HSV1-sr39tk provides greater sensitivity to imaging compared with the wild-type HSV1-tk (38). However, it is conceivable that the majority of progenitor cells after i.v. injection into murine hosts that had not been bone marrow ablated do not engraft into bone marrow or other organs and do not proliferate to produce progeny tissues to the degree that is biologically significant; they remain dormant throughout the organism, or the majority of these cells undergo apoptosis, especially after xenotransplantation.

Our *in vivo* PET imaging observations were cross-validated by *in situ* and *in vitro* analyses. Specifically, the immunocytofluorometric analyses of tumors confirmed the presence of EGFP$^+$ progeny cells differentiated into endothelial cells of tumor capillaries and small blood vessels, hair follicle cells, and basal cells of dermis overlaying the s.c. tumor xenografts. The later observations may be explained, at least in part, by the capacity of stem cells to nonspecifically home into the sites of tissue damage and inflammation (39), which are often observed in the skin overlaying s.c. tumors.

Previously, it was shown that MSCs have the propensity to differentiate as osteogenic, chondrogenic, adipogenic, and neurogenic lineages *in vitro* (29, 40). It is not known if transdifferentiation from hMSC to epithelial cells at the tumor site could involve mechanisms, such as the recently reported *in vitro* fusion of hMSC with heat-shocked epithelial cells (9). These differentiated tracer hMSC-derived progeny cells had exhibited a limited capacity for self-renewal as evidenced from the retransplantation experiments we did. One possible explanation of these results is that HSV1-TK$^+$, GFP$^+$ tracer stem cells, which contributed to the development of the tumor stroma in the original host, subsequently diminished their proliferative capacity due to differentiation, which was also evident from our *in vitro* replating experiments. Another possible explanation is that by 4 weeks after transplantation into the new host the HSV1-TK$^+$, GFP$^+$ tracer stem cells from the transplanted tumor tissue became "diluted" within the newly developing tumor stroma and/or were substituted by the recipient host-derived stroma-forming cells. Similar results on limited renewal capacity and <2-week life span of tumor-derived endothelial cells in retransplanted tumors have been reported previously (41).

In conclusion, we believe that the current study is first to provide the direct evidence for microscopic tumor targeting by exogenously administered hMSCs. The i.v. administered HSV1-TK-expressing tracer hMSCs can be used for noninvasive monitoring of stem cell–based therapies using whole-body PET imaging with [^{18}F]-FHBG or other HSV1-TK-specific radiotracers [^{18}F]-FEAU and [^{18}F]-FFAU (37, 42) or ^{124}I-FAIU (43, 44). It is also conceivable that PET imaging of i.v. administered HSV1-TK$^+$ tracer hMSCs can be exploited as a novel approach for noninvasive detection of otherwise radiologically nondetectable microscopic tumors and for monitoring the formation of HSV1-tk-expressing tumor stroma for ganciclovir therapy.

Acknowledgments

We thank Dr. Lung-Ji Chang (University of Florida) for supplying the original lentiviral vector system, Dr. H.E. Wang (National Yang-Min Medical University, Taipei) for the synthesis of FHBG precursor, and Dr. Otto O. Yang (University of California at Los Angeles) for editorial assistance.

References

1. Folkman J. Tumor angiogenesis: therapeutic implications. N Engl J Med 1971;285:1182–6.
2. Holash J, Maisonpierre PC, Compton D, et al. Vessel cooption, regression, and growth in tumors mediated by angiopoietins and VEGF. Science 1999; 284:1994–8.
3. Carmeliet P, Jain RK. Angiogenesis in cancer and other diseases. Nature 2000;407:249–57.
4. De Palma M, Venneri MA, Roca C, Naldini L. Targeting exogenous genes to tumor angiogenesis by transplantation of genetically modified hematopoietic stem cells. Nat Med 2003;9:789–95.
5. Prockop DJ. Marrow stromal cells as stem cells for nonhematopoietic tissues. Science 1997;276:71–4.
6. Pittenger MF, Mackay AM, Beck SC, et al. Multilineage potential of adult human mesenchymal stem cells. Science 1999;284:143–7.
7. Bruder SP, Fink DJ, Caplan AI. Mesenchymal stem cells in bone development, bone repair, and skeletal regeneration therapy. J Cell Biochem 1994;56:283–94.
8. Jin HK, Carter JE, Huntley GW, Schuchman EH. Intracerebral transplantation of mesenchymal stem cells into acid sphingomyelinase-deficient mice delays the onset of neurological abnormalities and extends their life span. J Clin Invest 2002;109:1183–91.
9. Spees JL, Olson SD, Ylostalo J, et al. Differentiation, cell fusion, and nuclear fusion during *ex vivo* repair of epithelium by human adult stem cells from bone marrow stroma. Proc Natl Acad Sci U S A 2003;100: 2397–402.
10. Reyes M, Dudek A, Jahagirdar B, et al. Origin of endothelial progenitors in human postnatal bone marrow. J Clin Invest 2002;109:337–46.
11. Orlic D, Kajstura J, Chimenti S, et al. Bone marrow cells regenerate infarcted myocardium. Nature 2001; 410:701–5.
12. Studeny M, Marini FC, Champlin RE, et al. Bone marrow-derived mesenchymal stem cells as vehicles for interferon-β delivery into tumors. Cancer Res 2002;62:3603–8.
13. Nakamura K, Ito Y, Kawano Y, et al. Antitumor effect of genetically engineered mesenchymal stem cells in a rat glioma model. Gene Ther 2004;11:1155–64.
14. Doubrovin M, Ponomarev V, Beresten T, et al. Imaging transcriptional regulation of p53-dependent genes with positron emission tomography *in vivo*. Proc Natl Acad Sci U S A 2001;98:9300–5.
15. Jacobs A, Dubrovin M, Hewett J, et al. Functional coexpression of HSV-1 thymidine kinase and green fluorescent protein: implications for noninvasive imaging of transgene expression. Neoplasia 1999; 1:154–61.
16. Ray P, Wu AM, Gambhir SS. Optical bioluminescence and positron emission tomography imaging of a novel fusion reporter gene in tumor xenografts of living mice. Cancer Res 2003;63:1160–5.
17. Ray P, De A, Min JJ, et al. Imaging tri-fusion multimodality reporter gene expression in living subjects. Cancer Res 2004;64:1323–30.
18. Chen WS, Wei SJ, Liu JM, et al. Tumor invasiveness and liver metastasis of colon cancer cells correlated with cyclooxygenase-2 (COX-2) expression and inhibited by a COX-2-selective inhibitor, Etodolac. Int J Cancer 2001;91:894–9.
19. Hung SC, Yang DM, Chang CF, et al. Immortalization without neoplastic transformation of human mesenchymal stem cells by transduction with HPV16 E6E7 genes. Int J Cancer 2004;110:313–9.
20. Chang LJ, Zaiss AK. Lentiviral vectors. Preparation and use. Methods Mol Med 2002;69:303–18.
21. Zaiss AK, Son S, Chang LJ. RNA 3′ readthrough of oncoretrovirus and lentivirus: implications for vector safety and efficacy. J Virol 2002;76:7209–19.
22. Tjuvajev JG, Doubrovin M, Akhurst T, et al. Comparison of radiolabeled nucleoside probes (FIAU, FHBG, and FHPG) for PET imaging of HSV1-tk gene expression. J Nucl Med 2002;43:1072–83.
23. Deng WP, Yang WK, Lai WF, et al. Non-invasive *in vivo* imaging with radiolabelled FIAU for monitoring cancer gene therapy using herpes simplex virus type 1 thymidine kinase and ganciclovir. Eur J Nucl Med Mol Imaging 2004;31:99–109.
24. Fareed MU, Moolten FL. Suicide gene transduction sensitizes murine embryonic and human mesenchymal stem cells to ablation on demand: a fail-safe protection against cellular misbehavior. Gene Ther 2002; 9:955–62.
25. Shiue GG, Shiue CY, Lee RL, et al. A simplified one-pot synthesis of 9-[(3-[^{18}F]fluoro-1-hydroxy-2-propoxy)methyl]guanine ([^{18}F]FHPG) and 9-(4-[^{18}F]fluoro-3-hydroxymethylbutyl)guanine ([^{18}F]FHBG) for gene therapy. Nucl Med Biol 2002;28:875–83.
26. Lee K, Kinahan PE, Fessler JA, et al. Pragmatic fully 3D image reconstruction for the MiCES mouse imaging PET scanner. Phys Med Biol 2004;49:4563–78.
27. Jockusch H, Voigt S, Eberhard D. Localization of GFP in frozen sections from unfixed mouse tissues: immobilization of a highly soluble marker protein by formaldehyde vapor. J Histochem Cytochem 2003; 51:401–4.
28. St Croix B, Rago C, Velculescu V, et al. Genes expressed in human tumor endothelium. Science 2000;289:1197–202.
29. Hung SC, Chen NJ, Hsieh SL, et al. Isolation and characterization of size-sieved stem cells from human bone marrow. Stem Cells 2002;20:249–58.
30. Miyagawa M, Anton M, Haubner R, et al. PET of cardiac transgene expression: comparison of 2 approaches based on herpesviral thymidine kinase reporter gene. J Nucl Med 2004;45:1917–23.
31. Wu JC, Chen IY, Sundaresan G, et al. Molecular imaging of cardiac cell transplantation in living animals using optical bioluminescence and positron emission tomography. Circulation 2003;108:1302–5.
32. Dubey P, Su H, Adonai N, et al. Quantitative imaging of the T cell antitumor response by positron-emission tomography. Proc Natl Acad Sci U S A 2003;100: 1232–7.
33. Koehne G, Doubrovin M, Doubrovina E, et al. Serial *in vivo* imaging of the targeted migration of human HSV-TK-transduced antigen-specific lymphocytes. Nat Biotechnol 2003;21:405–13.
34. Su H, Forbes A, Gambhir SS, Braun J. Quantitation of cell number by a positron emission tomography reporter gene strategy. Mol Imaging Biol 2004;6: 139–48.
35. Aboody KS, Brown A, Rainov NG, et al. Neural stem cells display extensive tropism for pathology in adult brain: evidence from intracranial gliomas. Proc Natl Acad Sci U S A 2000;97:12846–51.
36. Relf M, LeJeune S, Scott PA, et al. Expression of the angiogenic factors vascular endothelial cell growth factor, acidic and basic fibroblast growth factor, tumor growth factor β-1, platelet-derived endothelial cell growth factor, placenta growth factor, and pleiotrophin in human primary breast cancer and its relation to angiogenesis. Cancer Res 1997;57:963–9.
37. Serganova I, Doubrovin M, Vider J, et al. Molecular imaging of temporal dynamics and spatial heterogeneity of hypoxia-inducible factor-1 signal transduction activity in tumors in living mice. Cancer Res 2004; 64:6101–8.
38. Gambhir SS, Bauer E, Black ME, et al. A mutant herpes simplex virus type 1 thymidine kinase reporter gene shows improved sensitivity for imaging reporter gene expression with positron emission tomography. Proc Natl Acad Sci U S A 2000; 97:2785–90.
39. Cottler-Fox MH, Lapidot T, Petit I, et al. Stem Cell Mobilization. Hematology (Am Soc Hematol Educ Program) 2003:419–37.
40. Hung SC, Cheng H, Pan CY, et al. *In vitro* differentiation of size-sieved stem cells into electrically active neural cells. Stem Cells 2002;20:522–9.
41. Duda DG, Fukumura D, Munn LL, et al. Differential transplantability of tumor-associated stromal cells. Cancer Res 2004;64:5920–4.
42. Alauddin MM, Shahinian A, Park R, et al. Synthesis and evaluation of 2′-deoxy-2′-^{18}F-fluoro-5-fluoro-1-β-D-arabinofuranosyluracil as a potential PET imaging agent for suicide gene expression. J Nucl Med 2004; 45:2063–9.
43. Tjuvajev JG, Avril N, Oku T, et al. Imaging herpes virus thymidine kinase gene transfer and expression by positron emission tomography. Cancer Res 1998; 58:4333–41.
44. Wen B, Burgman P, Zanzonico P, et al. A preclinical model for noninvasive imaging of hypoxia-induced gene expression; comparison with an exogenous marker of tumor hypoxia. Eur J Nucl Med Mol Imaging 2004;31:1530–8.